



# Experimental investigation on mechanical characteristics of red sandstone under graded cyclic loading and its inspirations for stability of overlying strata

Qican Ran · Yunpei Liang · Quanle Zou ·  
Yang Hong · Bichuan Zhang · Hao Liu ·  
Fanjie Kong

Received: 23 April 2022 / Accepted: 6 November 2022  
© The Author(s) 2023

**Abstract** The horizontal stress in the fractured blocks of a fractured zone is in a stress relief status under repeated mining disturbances. To investigate the effect of the horizontal stress in fractured blocks on the stability of the overlying strata, uniaxially graded cyclic loading and unloading experiments on red sandstone with different initial stress level were carried out. First, the evolution of the loading and unloading elastic modulus, irreversible strain and load-unload response ratio were analyzed. Then, the strain energy evolution and damage variable characteristics were examined. Finally, the stability of a

voussoir beam structure under repeated mining disturbances was discussed. The results showed that with increasing cycle number, the elastic modulus showed a nonlinear decreasing trend, the load-unload response ratio always fluctuated at approximately 1, and the irreversible strain showed a rapid and steady increasing trend. The proportion of elastic energy tended to increase linearly with increasing cycle number, while the proportion of dissipated strain energy tended to decrease. Moreover, the damage variable, based on the dissipation strain energy definition, showed a parabolic growth trend with increasing cycle number. The irreversible strain and damage variables showed an “increasing–decreasing–increasing” trend as the initial stress level increased. Finally, a stability criterion of the voussoir beam structure based on the effect of repeated mining disturbances on horizontal thrust was proposed. This research has important implications for overlying strata stability.

---

Q. Ran · Y. Liang (✉) · Q. Zou (✉) · Y. Hong ·  
B. Zhang · F. Kong  
State Key Laboratory of Coal Mine Disaster Dynamics  
and Control, Chongqing University, Chongqing 400044,  
China  
e-mail: liangyunpei@126.com

Q. Zou  
e-mail: quanlezou2011@126.com

Q. Ran · Y. Liang · Q. Zou · Y. Hong · B. Zhang · F. Kong  
School of Resources and Safety Engineering, Chongqing  
University, Chongqing 400044, China

H. Liu  
Chongqing Key Laboratory of Heterogeneous Material  
Mechanics, Chongqing University, Chongqing 400044,  
China

H. Liu  
College of Aerospace Engineering, Chongqing University,  
Chongqing 400044, China

## Article highlights

- (1) The mechanical characteristics of red sandstone under graded cyclic unloading were elucidated.
- (2) The stability characteristics of overlying strata under repeated mining disturbances were analyzed.
- (3) A stability criterion of the voussoir beam structure in overlying strata under repeated mining was proposed.

**Keywords** Red sandstone · Cyclic loading · Mechanical characteristics · Voussoir beam structure · Overlying strata

## 1 Introduction

Rock materials are one of the most widely used materials in engineering (Kong et al. 2016; Yang 2016; Liu et al. 2020; Zou et al. 2022a); they are commonly used in many fields (Li et al. 2017; Zhang et al. 2022a; Zou et al. 2021), such as mining engineering, and underground engineering. Among them, the loading on the overlying strata under a mining disturbance is essentially cyclic loading, and the mechanical properties under cyclic loading are an important influence on the stability of the rock mass. (Cerfontaine and Collin 2018; Hao et al. 2020; Xiao et al. 2020). In addition, in the coal mining process, mining disturbances usually result in a complex stress state of the rock mass (Zhang et al. 2020). For example, under a mining disturbance, the intact rock of the overlying strata can fracture into intact blocks of different sizes, forming a fractured zone (Zhang et al. 2019a). In coal seam mining (Fig. 1), after the fracture of the key strata in the overlying strata, the fractured block below the delamination fracture in the fractured zone may form voussoir beam structure (VBS) or cantilever beam structure (Zhao et al. 2022). At this time, the vertical force and horizontal friction force on the fractured block are almost negligible compared with

the horizontal force. Similar to this situation is the soft roof collapse phenomenon in longwall mining of shallow buried coal seams (Suchowerska et al. 2014; Zhao et al. 2018). In longwall mining of shallow buried coal seams, the roof plate is prone to collapse when a weak roof plate and a high horizontal stress exist at the same time (Zhang et al. 2019b, 2022b). At this time, the coal seam is shallow, and the vertical stress is negligible compared to the high horizontal stress. Therefore, the specific fractured block of overlying strata is in an approximately uniaxially compressed state (Zhu et al. 2019; Xia et al. 2021). With mining disturbances, the vertical stress on the overlying strata gradually increases, and the horizontal stress gradually decreases; during the mining process of repeated seams, specific fractured blocks experience different disturbances and continuous stress release (Wu et al. 2021). The horizontal stress on the fractured block gradually decreases in this region, which shows a decreasing graded amplitude cyclic loading and unloading. Therefore, investigating the mechanical properties of fractured blocks under cyclic loading is important, which can provide a reference for the stability of the overlying strata structure.

At present, a large number of loading experiments have been conducted, including cyclic loading experiments under different stress path, different prefabricated crack and other conditions (Zhu et al. 2020; Zhao et al. 2021a; Liang et al. 2022; Zou et al. 2022b). For example, true triaxial loading experiments on marble have been conducted to elucidate

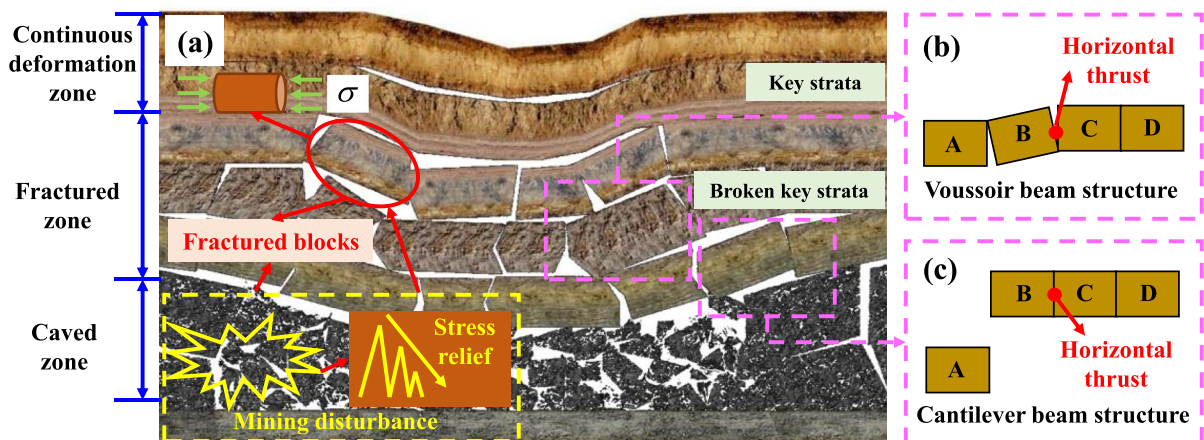


**Fig. 1** Distribution of blocks in the fractured zone. (a) Schematic diagram of overlying strata under a mining disturbance; (b) voussoir beam structure; and (c) cantilever beam structure

the properties of the mechanical parameters of specimens, such as residual deformation and strain energy, during the cyclic process (Gao and Feng 2019). Cyclic loading and unloading experiments on sandstone, marble, and granite have been conducted to elucidate the variation in rock mechanical properties with accumulated damage (Feng et al. 2020). Tian et al. (2021) elucidated the properties of thermally treated granite, which is more susceptible to failure under cyclic loading, through triaxial compression experiments. Meng et al. (2021a) found a hysteresis effect in the specimen stress–strain evolution curve and a relationship between the evolution of the deformation parameters and the number of cycles in the limestone cyclic loading experiments. In addition, cyclic loading waveforms show different patterns (Le et al. 2014). The most common waveforms are sine, linear, and square waves; among them, square waves are the most destructive, and linear variations are the least destructive (Whittles et al. 2007).

Currently, most cyclic loading experiments use constant amplitude or incremental loading paths, with a focus on rock fatigue or failure-related hazards (Fu et al. 2020; Li et al. 2020). However, the effects of horizontal thrust between fractured blocks have rarely been investigated to locate the stress release pattern in fractured zones. The stable structure formed by fractured blocks in the overlying strata involves the stress relief, deformation and damage behavior of the fractured block (Wei et al. 2020; Zhang and Wang 2021). The magnitude of the initial horizontal thrust influences the mechanical properties of the fractured block and the stability of the VBS. Therefore, the mechanical behavior of fractured blocks under cyclic loading at different initial stress level (ISL) has an important impact on the VBS. However, the effects of different ISL on the mechanical response of fractured blocks are still unclear.

In summary, an investigation and analysis of the mechanical characteristics of fractured blocks on the stability of the VBS is essential to investigate the stability of the overlying strata. Therefore, the mechanical characteristics of fractured blocks with cyclic loading at different ISL were analyzed, and the effects of repeated mining disturbances on the stability of the VBS were explored. First, the evolutionary characteristics of the elastic modulus, irreversible strain and load-unload response ratio were analyzed by using stress–strain curves. Then, the elastic and dissipative

strain energies were calculated, and the strain energy evolution was analyzed. Subsequently, the damage characteristics of the fractured block were obtained based on the dissipative strain energy. Finally, a stability criterion for a VBS considering the effects of repeated mining disturbances on horizontal thrust is proposed.

## 2 Experimental methods

### 2.1 Red sandstone specimens

The specimens of red sandstone were taken from the same complete rock, and the specimens were made into  $\varnothing 50 \text{ mm} \times 100 \text{ mm}$  cylindrical specimens. Prior to the experiments, the red sandstone specimens were screened for quality and P-wave velocity to ensure that the selected specimens had relatively similar mechanical properties. The red sandstone specimens used for the experiments were stored at a room temperature of approximately 25 degrees. The quality and P-wave velocity of red sandstone specimens are as follows (Table 1).

Before formal experiments were started, the uniaxial compressive strength (UCS) of red sandstone was tested by conducting two sets of uniaxial compression experiments. The results of the two measurements are shown in Table 2. The average value of 52.86 MPa of the results was taken as the UCS of the red sandstone specimens.

### 2.2 Experimental instrument and method

The experiments were conducted using the “micro-computer-controlled electronic universal experiment machine” of the College of Aerospace Engineering,

**Table 1** The quality and P-wave velocity of the experimental specimens

No	Quality (g)	P wave velocity (km/s)
#1	452.12	3.14
#2	453.02	3.16
#3	450.67	3.16
#4	451.45	3.11
#5	451.70	3.17

**Table 2** UCS measurement results of red sandstone specimens

No	Quality (g)	P wave velocity (km/s)	Uniaxial compressive strength (MPa)
UCS-#1	450.13	3.09	51.44
UCS-#2	451.29	3.18	54.28

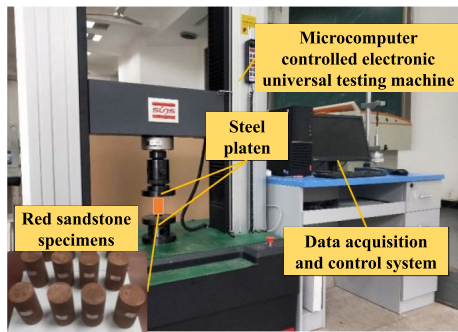


**Fig. 2** Experimental system of rock mechanics

Chongqing University, as shown in Fig. 2. The equipment can be used to obtain the compressive strength, axial deformation and other mechanical parameters. The equipment is driven by a servo motor, which drives the moving beam up and down through the transmission mechanism to realize the experimental loading process.

As shown in Fig. 3a, a decreasing graded amplitude cyclic loading experiment was performed with ISL set at 64, 72, 80, 88, and 96% of the UCS (33.8, 38.0, 42.2, 46.4, and 50.6 MPa, respectively), followed by two cycles of 20 graded amplitude reduction unloading stages with an unloading amplitude of 1% UCS. Finally, the loading was continued until the specimen failed. As shown in Fig. 3b, taking the ISL of 80% UCS as an example, the axial stress is cyclically unloaded from 80% UCS to 60% UCS in the 1st unloading stage, as follows: 80% → 60% → 79% → 60% → ..... → 60%. In the 2<sup>nd</sup> unloading stage, the axial stress is cyclically unloaded from 60% UCS to 40% UCS, and the specific cyclic steps are 60% → 40% → 59% → 40% → ..... → 40%. Throughout the experiment, the applied loading rate was 400 N/s. The specimens were numbered according to the experimental protocol. The specimens with ISL of 64, 72, 80, 88 and 96% UCS are specimens #1, #2, #3, #4, and #5, referred to as ISL-64%, ISL-72%, ISL-80%, ISL-88%, and ISL-96%, respectively.

### 3 Results

#### 3.1 Stress–strain curve evolution

The rock stress–strain curve represents the entire process of deformation and failure of the rock (Meng et al. 2020, 2021b). To make the stress–strain curve

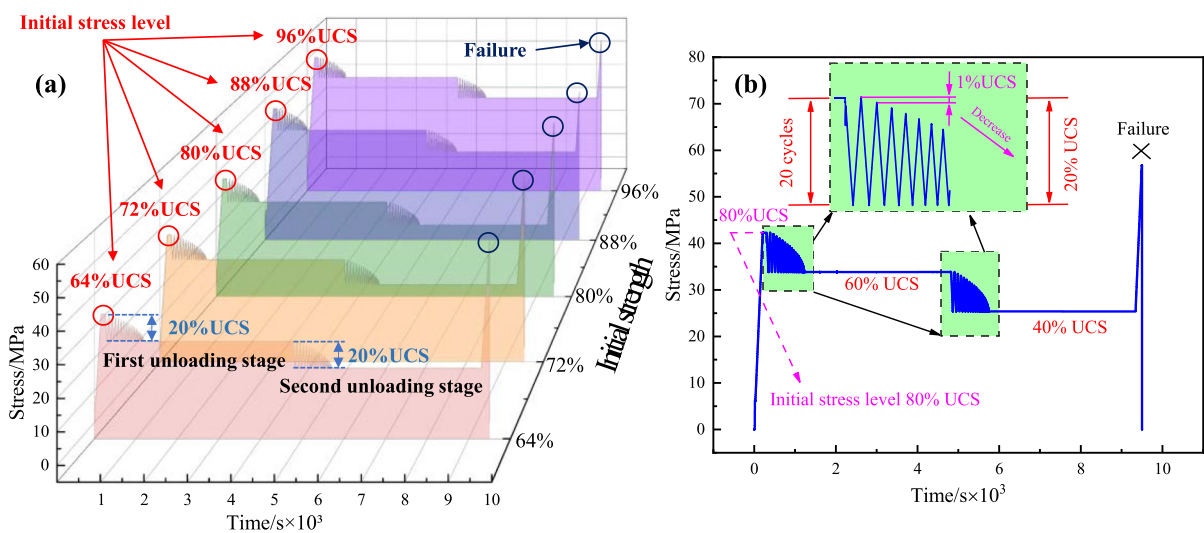


**Fig. 3** Stress path: (a) five experimental stress path diagrams and (b) a case of ISL-80%

more accurate, the displacement where the press head is not in contact with the specimen is not considered, but the actual force on the specimen is used as a starting point for plotting the stress–strain curve.

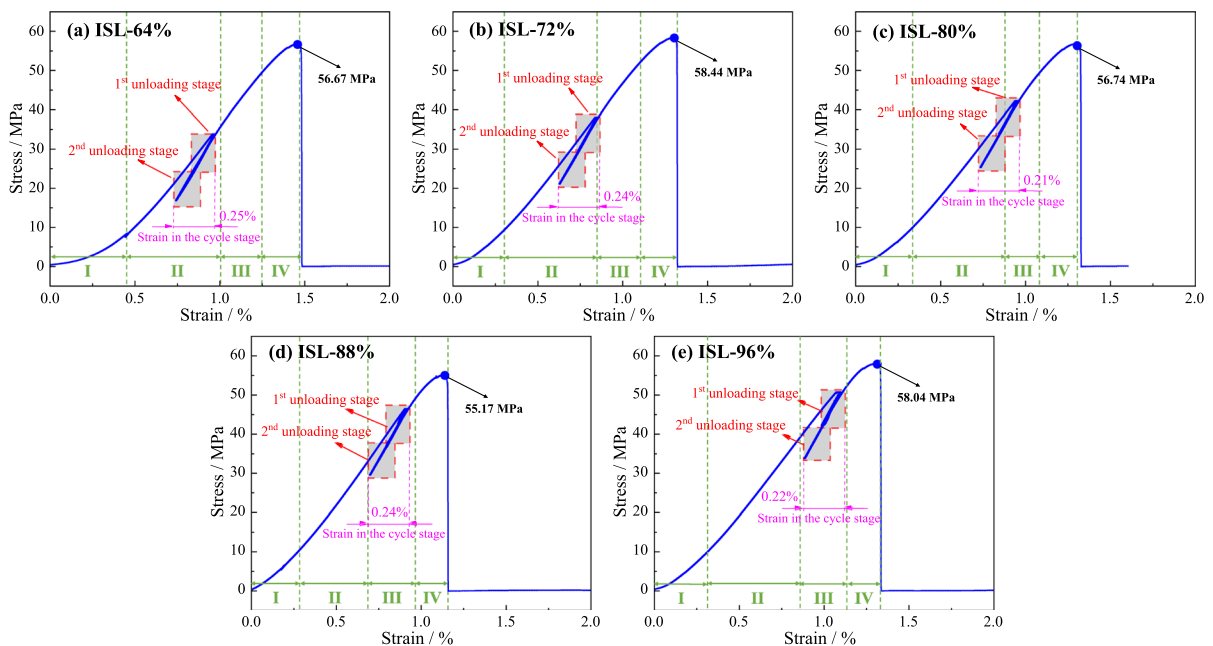
Figure 4 illustrates the stress–strain curves of red sandstone under cyclic loading with different ISL. In the prepeak stage, the stress–strain curve presents four phase characteristics, divided according to the slope of the curve (Zhang et al. 2022c). The four stages include the crack closure stage, the crack initiation stage, the crack damage stage and the unstable crack propagation stage. In the crack closure stage (stage I), the internal microfractures of red sandstone are gradually compacted under pressure. At this point, the stress–strain curve is upwardly concave. In the crack initiation stage (stage II), the internal microfractures of red sandstone specimens are closed, at which time the curve is linear and the deformation is recoverable. In the crack damage stage (stage III), the internal fractures of red sandstone develop, and new fractures appear, at which time the stress–strain is nonlinearly increasing and the specimens have irreversible deformation. In the unstable crack propagation stage (stage IV), with increasing loading, when the red sandstone specimen reaches the ultimate

compressive strength, the internal fractures penetrate each other, the red sandstone specimen fails, and the macroscopic rupture surface appears. At this point, the slope of the curve tends to decrease. As shown in Fig. 4, in all graded cyclic loading experiments, the red sandstone specimens failed at almost the same peak strength, and its peak strain was approximately 1.4%. In addition, it can also be found that the strain in the cyclic stage of the specimens was approximately 0.23%.

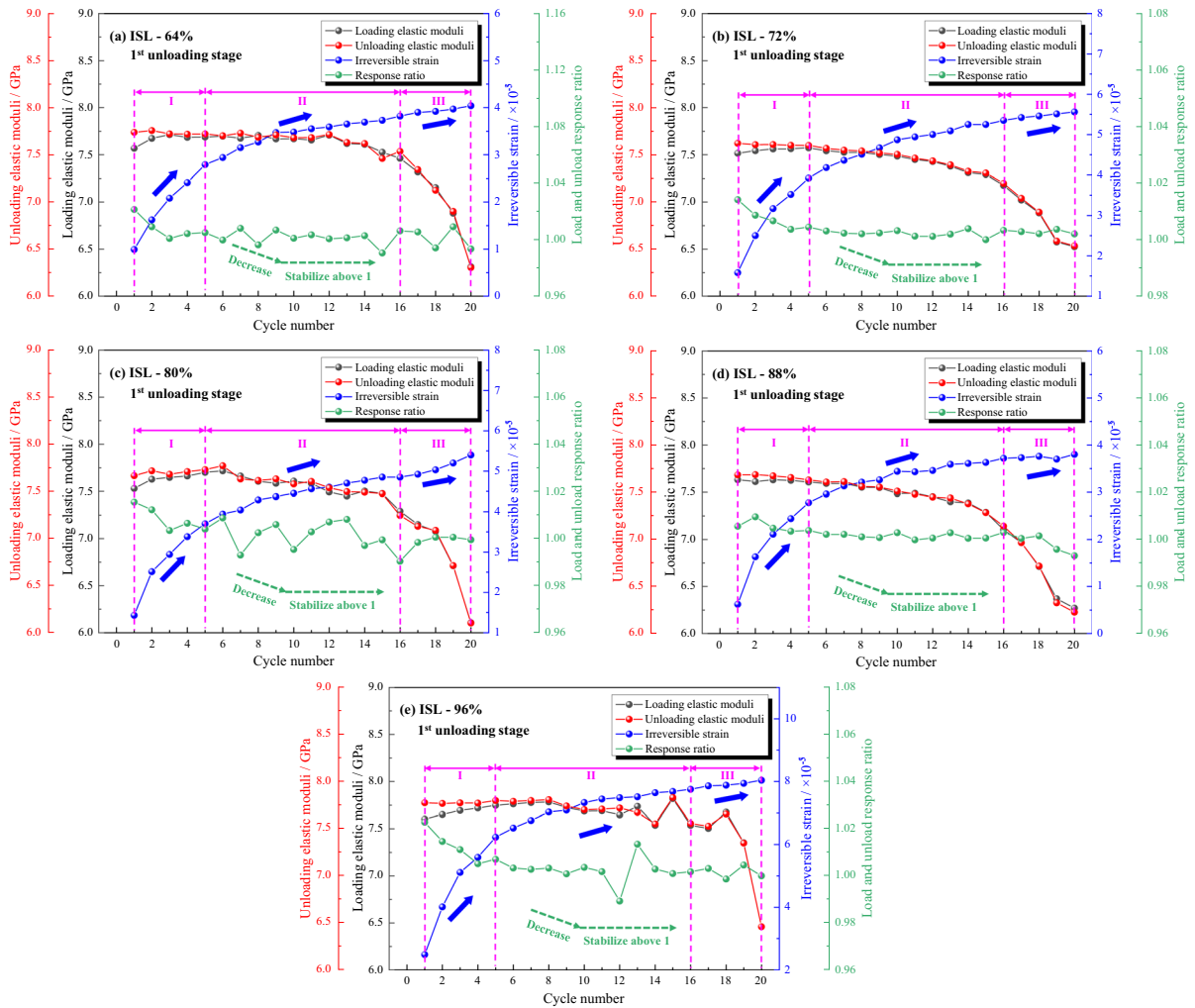
### 3.2 Elastic modulus, irreversible strain and load-unload response ratio characteristics

Figure 5 shows the relationship among the deformation parameters and cycle number for the 1<sup>st</sup> cyclic unloading stage of red sandstone at different ISL in the cyclic loading experiment.

The elastic modulus of specimens indicates the ability to resist deformation under loading and can characterize the fracture development and failure properties of specimens to some extent. Under different loading paths, the elastic modulus of rocks can show significant differences due to adverse effects such as hysteresis effects and unloading damage



**Fig. 4** Stress–strain curves of red sandstone under different ISL. (a) ISL-64%; (b) ISL-72%; (c) ISL-80%; (d) ISL-88%; and (e) ISL-96%



**Fig. 5** Deformation parameters versus cycle number for the 1st unloading stage at different ISL. (a) ISL-64%; (b) ISL-72%; (c) ISL-80%; (d) ISL-88%; and (e) ISL-96%

(Peng et al. 2019a). In Fig. 5, with increasing cycle number, the patterns of the loading and unloading elastic modulus were consistent, showing a decreasing trend, which is comparable to the results of previous authors (Arora et al. 2019). In addition, the loading elastic modulus was slightly smaller than the unloading elastic modulus during the cyclic unloading stage, which indicates the hardening effect caused by cyclic loading.

Natural rocks material have internal defects such as pores and fractures, which facilitate deformation. Under loading, rocks have elastic deformation and irreversible deformation (Peng et al. 2020). Among them, the calculation principle of the rock irreversible

strain is shown in Fig. 6. Equation (1) (Peng et al. 2019b) is used to calculate the irreversible strain.

$$\epsilon_{irr} = \sum_{n=1}^N \Delta \epsilon_{irr}^n = \sum_{n=1}^N (\epsilon_2^n - \epsilon_1^n) \tag{1}$$

where  $\epsilon_{irr}$  is the irreversible axial strain in total and single cycles and  $n$  is the number of cycles. In addition,  $\epsilon_2^n$  and  $\epsilon_1^n$  denote the final strain at the end of the cycle and the initial strain at the beginning of the cycle, respectively.

Figure 5 shows that the irreversible accumulated strain tended to increase with the increasing cycle number. Since this was the result of the 1<sup>st</sup> unloading

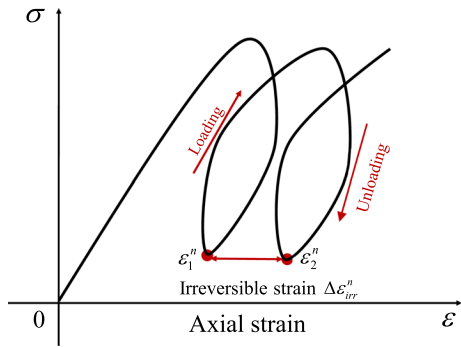


**Fig. 6** Principle of the irreversible strain calculation

stage, the irreversible strain was expressed in three stages (Peng et al. 2020): the initial rapid stage of strain increase (stage I), the stable stage of strain increase (stage II) and the accelerated stage of strain increase (stage III). Among them, the acceleration effect of stage III was not obvious, which may be due to the gradual decrease in the stress level and the small amplitude of unloading under cyclic loading. In addition, in the 1st unloading stage, the irreversible strain was 4.04, 5.56, 5.40, 3.80 and 8.04‰, corresponding to ISL-64%, ISL-72%, ISL-80%, ISL-88% and ISL-94%, respectively. The irreversible strain tends to "increase–decrease–increase" with increasing ISL.

The load-unload response ratio is a parameter that characterizes the damage of specimens based on stress–strain data. The calculation of the load-unload response ratio (Duan et al. 2020; Gong et al. 2019a) is as follows. The strain is used as the response quantity in the load-unload response ratio, and the load-unload response quantity is obtained based on the linear elastic instanton model relationship.

$$X = \lim_{\Delta P \rightarrow 0} \frac{\Delta R}{\Delta P} = \frac{\Delta \epsilon}{\Delta \sigma} = \frac{1}{E} \tag{2}$$

Then, the load-unload response ratio  $Y$  is

$$Y = \frac{X_+}{X_-} = \frac{1/E_+}{1/E_-} = \frac{E_-}{E_+} \tag{3}$$

where  $X$  is the load-unload response;  $\Delta R$  is the response change;  $\Delta P$  is the load change;  $X_+$  and  $X_-$  are the response of the loading and unloading sections, respectively;  $E_+$  and  $E_-$  are the elastic modulus of the loading and unloading sections, GPa,

respectively;  $\Delta \epsilon$  is the strain change; and  $\Delta \sigma$  is the stress change, MPa.

In Fig. 5, the overall decreasing trend of the load-unload response ratio was observed in the 1st unloading stage of the red sandstone. With increasing cycle number, the load-unload response ratio gradually fluctuated approximately 1 and stabilized above 1. This is probably because the initial high stress disturbance in the 1st unloading stage led to the high response ratio; with cyclic unloading, the stress level decreased, the small disturbance did not cause the failure of the red sandstone, and the internal stability of the specimen was high. Thus, the response ratio was small and finally stabilized above 1.

Figure 7 shows the relationship among the deformation parameters and cycle number for the 2nd cyclic unloading stage of red sandstone at different ISL. In the 2nd cyclic unloading stage, the loading and unloading elastic modulus was less variable but still showed a decreasing trend. As the cycle number increased, the red sandstone at lower stress levels also showed an increasing trend but only in two stages: the initial rapid stage of strain increase (stage I) and the stable stage of strain increase (stage II). Compared with the first cyclic unloading stage, accelerated stage III was less obvious, which may be due to the graded cyclic unloading path, where the internal fracture development and expansion of the specimen was much less than the cyclic loading path. In addition, in the 2nd unloading stage, the irreversible strain was 1.26, 1.70, 1.22, 1.29 and 3.28‰, corresponding to ISL-64%, ISL-72%, ISL-80%, ISL-88% and ISL-94%, respectively. The irreversible strain also tends to "increase–decrease–increase" with increasing ISL. Due to the lower stress levels, the specimens are less deformed compared to the 1st unloading stage. The load-unload response ratio showed a pattern of increasing first and then stabilizing below 1, which again indicated that the loading elastic modulus was slightly more pronounced than the unloading elastic modulus, and the variability was smaller.

### 3.3 Strain energy evolution

The entire experimental system is considered to be a system with no exchange of matter and energy with the outside world, which means that no heat, light, or other forms of energy release during the experiment.

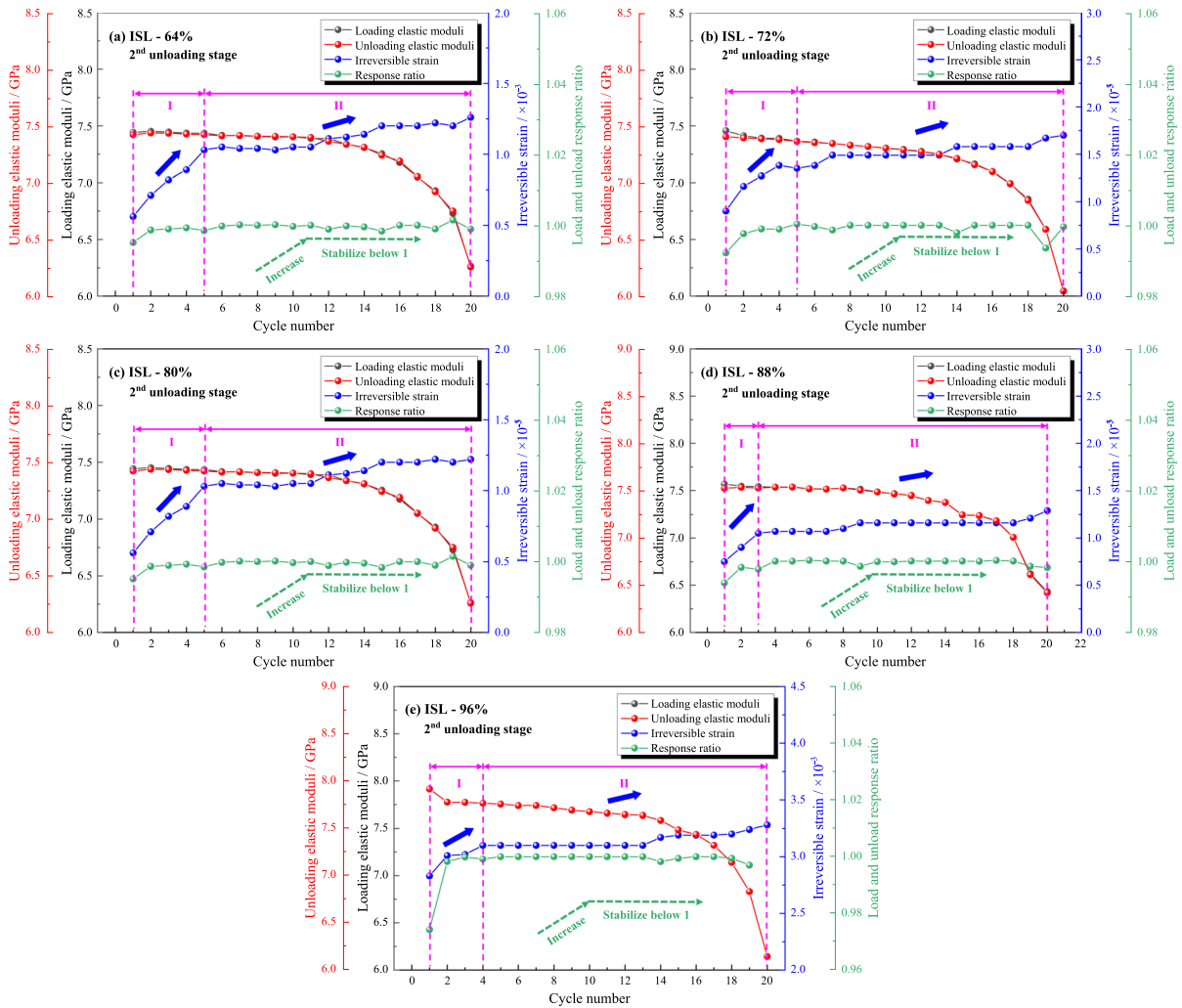


**Fig. 7** Deformation parameters versus cycle number for the 2nd unloading stage at different ISL. (a) ISL-64%; (b) ISL-72%; (c) ISL-80%; (d) ISL-88%; and (e) ISL-96%

Therefore, the total input strain energy  $U$  consists elastic strain energy  $U^e$  and dissipative strain energy  $U^d$  (Liu et al. 2021). The  $U$ ,  $U^e$  and  $U^d$  can be calculated for each cycle of the cyclic loading phase at different ISL (Chen et al. 2021). Figure 8 shows the calculation principle of strain energy. The strain energy calculation equation (Dou et al. 2020) is as follows.

$$U = \int_0^{\epsilon'} f_1(\epsilon) d\epsilon \tag{4}$$

$$U^e = \int_{\epsilon''}^{\epsilon'} f_2(\epsilon) d\epsilon \tag{5}$$

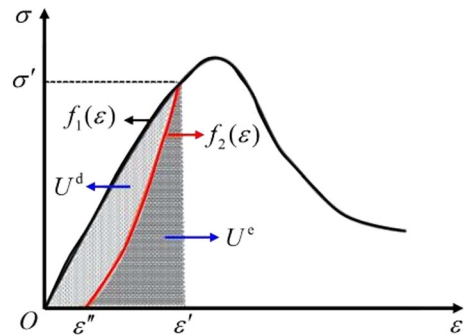


**Fig. 8** Principle of the strain energy calculation



$$U^d = U - U^e = \int_0^{\epsilon'} f_1(\epsilon) d\epsilon - \int_0^{\epsilon''} f_2(\epsilon) d\epsilon \quad (6)$$

where  $U$  is the total strain energy,  $\text{kJ/m}^3$ ;  $U^e$  is the releasable elastic strain energy stored per unit volume,  $\text{kJ/m}^3$ ; and  $U^d$  is the dissipated strain energy that forms the internal damage and plastic deformation of red sandstone,  $\text{kJ/m}^3$ .

According to the Eqs. (4), (5) and (6), the strain energy of red sandstone during cyclic loading can be calculated, and then the percentage of  $U^e$  and  $U^d$  of each cycle can be obtained.

Figure 9 shows the strain energy evolution curve of red sandstone in the 1<sup>st</sup> cyclic unloading stage. The total strain energy tended to decrease with the increasing cycle number. This was due to the significant compression-density effect, large deformation at the beginning of the cycle, and increased strain energy input. With graded cycle unloading, the stress level gradually decreased, and the deformation was relatively small; thus, the experimental machine did less work on the red sandstone, and the total strain energy input decreased. With increasing cycle number, the  $U^e$  showed a smooth trend

in general. Most of the  $U$  was stored inside the red sandstone in the form of  $U^e$ , and the proportion of  $U^e$  to  $U$  showed a linear increasing trend. Notably, the  $U^e$  accounted for more than 95% under graded cyclic unloading. This indicated that most of the strain energy input in the experiment was used for the accumulation of  $U^e$ . The evolution pattern of  $U^d$  and its percentage was similar to that of  $U$ , showing a decreasing trend. This was because the initial rock fracture compacting effect gradually decreased with graded cyclic unloading, and the  $U^d$  used for fracture extension penetration gradually decreased.

Figure 10 illustrates the strain energy evolution curve of the red sandstone in the 2nd cyclic unloading stage. Similar to the 1st cyclic unloading stage, the  $U$  showed a decreasing trend with increasing cycle number, and the  $U^e$  showed a smooth trend in general. Notably, the proportion of  $U^e$  to  $U$  showed an increasing trend with a nearly linear relationship. The evolution pattern of  $U^d$  and its percentage was similar to that of the  $U$ , showing a decreasing trend. Slightly different from the 1st cyclic unloading stage, the strain energy evolution was strongly linearly related in this lower stress phase.

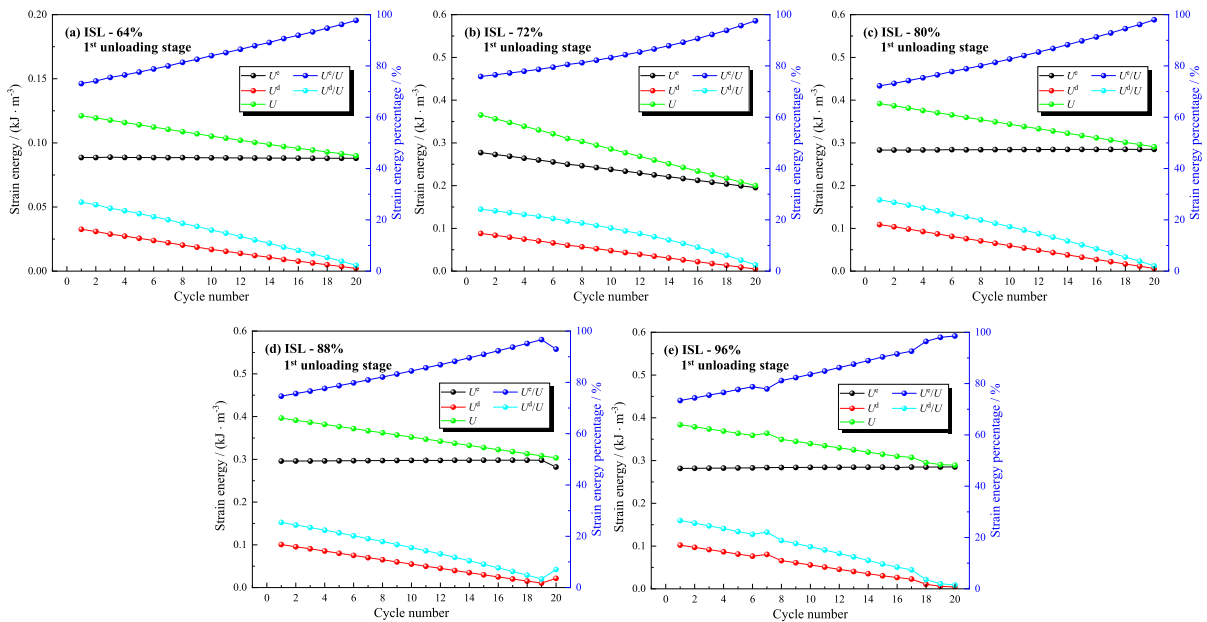


**Fig. 9** Strain energy evolution curves of red sandstone in the 1st cyclic unloading stage. (a) ISL-64%; (b) ISL-72%; (c) ISL-80%; (d) ISL-88%; and (e) ISL-96%

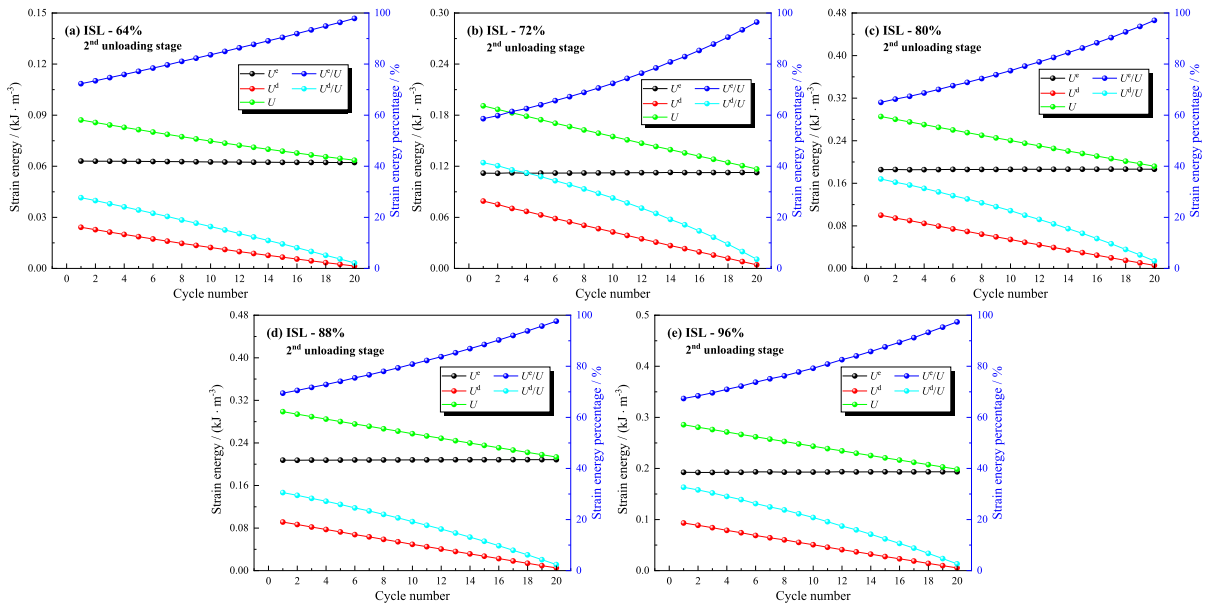


**Fig. 10** Strain energy evolution curves of red sandstone in the 2nd cyclic unloading stage. (a) ISL-64%; (b) ISL-72%; (c) ISL-80%; (d) ISL-88%; and (e) ISL-96%

### 3.4 Damage variable characteristics

For the characterization of damage variables, at present, based on stress–strain curves, damage variable expressions can be established from the perspectives of elastic modulus, plastic strain, and energy density. However, since natural rock have original defects and non-linear characteristics, the damage variables defined by the elastic modulus and plastic strain are prone to anomalies of reduction. Therefore, dissipated strain energy was used to define in this research. The ratio of the dissipated strain energy accumulated in the  $i^{\text{th}}$  cycle to the total input strain energy in the final stage is defined as the damage variable. The expression of the damage variable is as follows (Liu et al. 2018).

$$D_i = \frac{\sum_{i=1}^N U_i^d}{U} \quad (7)$$

where  $D_i$  is the damage variable of the  $i^{\text{th}}$  cycle;  $U_i^d$  is the dissipated strain energy of the rock under the  $i^{\text{th}}$  cyclic loading,  $\text{kJ}/\text{m}^3$ ; and  $U$  is the total input strain energy of the rock under the cyclic load,  $\text{kJ}/\text{m}^3$ .

Figure 11a and b show the damage variable evolution curves of red sandstone in two cyclic stages under graded cyclic unloading. As the cycle number increased, the damage variable evolution curve showed a parabolic trend. The damage variable increases faster in the early stages and then increases slowly. This was due to the stress level was high during the early stage of cycling loading, and the internal fracture development of the specimen was obvious. With graded cyclic unloading, the internal fracture development of the specimen was slow, the damage level was small, and the internal damage accumulation increased slowly.

Due to the compression-density effect of the red sandstone at the beginning of loading, the internal fracture development of the specimens in the first few cycles was more obvious, the energy dissipation was larger, and the damage was larger. As the cyclic stress decreased, the energy dissipation decreased, the variation of damage variables in per cycle was smaller, and the damage accumulated slowly. From Fig. 11a and b, the two stages of the damage variable with increasing ISL showed an “increase–decrease–increase” trend. This is in accordance with the previous trend of

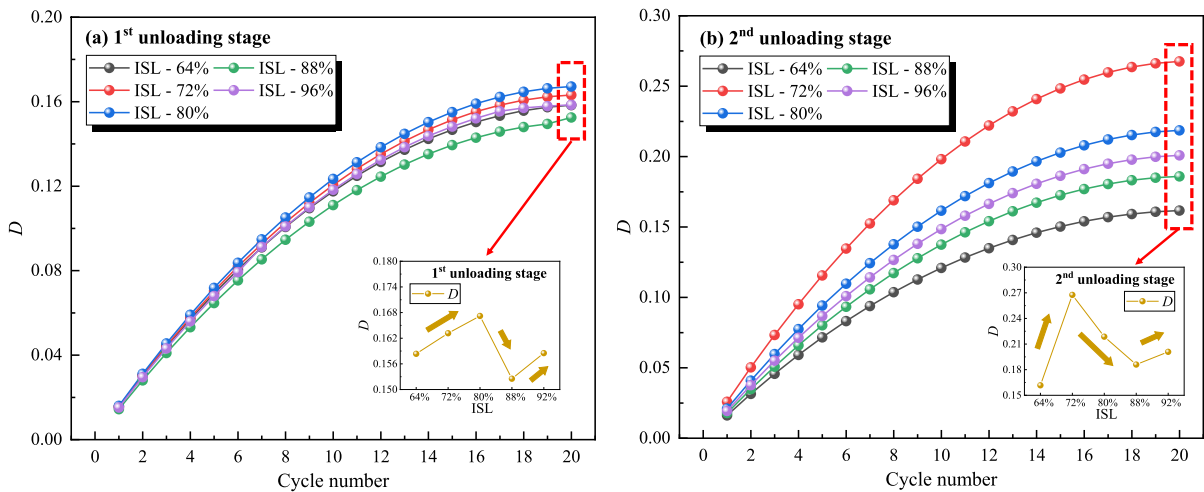


**Fig. 11** Damage variable evolution curves. (a) 1st cyclic unloading stage and (b) 2nd cyclic unloading stage

irreversible strain. This indicated that the ISL and the damage variable had a certain relationship and demonstrated a “wave-like” increasing trend, with peaks and valleys. After reaching a peak, the damage variable decreased with the ISL; then, after reaching a valley, the damage variable increased.

## 4 Discussion

### 4.1 Mechanical characteristics of red sandstone under graded cyclic unloading

In underground mining or geotechnical engineering, the stress perturbations in rocks are usually not constant but vary periodically (Wang et al. 2021). With activities such as coal mining, the stress in rocks usually increases (Wang et al. 2020). However, the fractured blocks of the overlying strata under repeated mining experience a cyclic release of horizontal stresses (Qu et al. 2015). This is critical for research on overlying strata movement. Therefore, in this research, graded cyclic loading and unloading experiments with decreasing amplitudes at different ISL of red sandstone were conducted. The experimental results showed that different ISL had an impact on the mechanical characteristics of the red sandstone and had a more apparent impact on the irreversible strain and strain energy evolution characteristics, which was similar to the results of previous research on the mechanical response of rock (Gong et al. 2019b).

Due to the extremely complex mechanical state of rocks in a real environment, it is difficult to develop a general theory to accurately model and predict the mechanical properties (Renani and Cai 2021). Therefore, the investigation is usually carried out by extracting the corresponding stress paths with simplified stress states. For this research, the following interesting results were obtained. The loading and unloading elastic modulus showed a nonlinear decreasing trend, and the load-unload response ratio demonstrated an opposite trend for the 1st and 2nd stages. This could be because the damage inside the red sandstone in the 1st cyclic unloading stage was greater than that in the 2nd cyclic unloading stage. In addition, the irreversible strain varied in a similar manner to that of the previous results (Zhao et al. 2021b), but its deformation was small, and the accelerated stage of strain increase (stage III) did not appear in the 2nd cyclic unloading. Moreover, the irreversible strain and damage variable showed an “increase–decrease–increase” trend with increasing ISL, which is a very interesting discovery.

As shown in Fig. 12, the horizontal stress on the fractured blocks gradually decreases as the mining of the coal seam progresses, showing a graded cyclic loading and unloading with decreasing amplitude. The results showed that the irreversible strain and damage variables change with increasing ISL, showing an “increasing–decreasing–increasing” trend and a threshold effect. In addition, fractured blocks form a stable VBS under mining disturbances. The experimental results provide some inspirations into

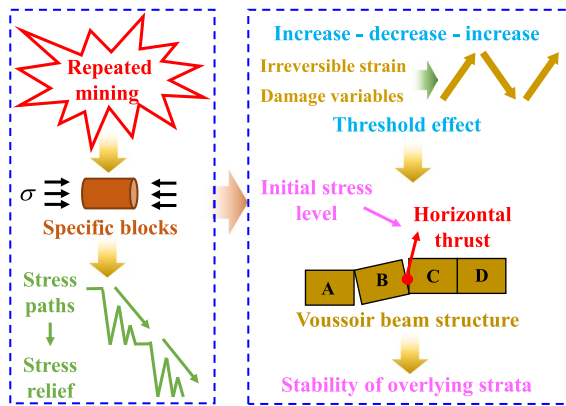


**Fig. 12** Implications of the experimental results for the stability of overlying strata

the stability of the overlying strata. There is a certain threshold for the value of the ISL, which affects the stability of the VBS. Under repeated mining disturbances, the horizontal stress gradually decreases to a point where it is impossible to maintain the stability of the VBS.

#### 4.2 Analysis of forces in overlying strata under mining disturbances

As shown in Fig. 13, under a single mining disturbance, the overlying strata forms “three vertical zones”: caved zone, fractured zone and continuous deformation zone. Laterally, there are also “three horizontal zones”: coal wall support zone A, delamination zone B and recompaction zone C (Han 2021). Among them, the fractured block of the

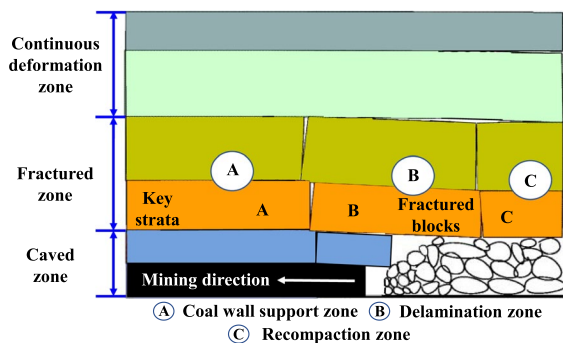


**Fig. 13** Stress analysis of the overlying strata under mining disturbances

key strata in the fractured zone forms a VBS (Liang et al. 2017), as shown in Fig. 13.

In today’s situation where coal mining extends deeper with repeated mining of coal seam groups, it is essential to introduce the impact of repeated mining disturbances based on the VBS and coal mining conditions. Repeated mining disturbances can cause changes in the horizontal thrust, these changes can lead to the instability of the VBS, which in turn leads to the instability of the overlying strata structure (Feng et al. 2019), as shown in Fig. 14.

In Fig. 15,  $P_B$  and  $P_C$  are the loads borne by key blocks B and C in the overlying strata,  $\text{kN/m}^2$ ;  $\theta_1$  and  $\theta_2$  are the rotation angles of key blocks B and C;  $W_1$ ,  $W_2$  are the amount of block B and block C underlayment, mm;  $Q_B$  and  $Q_C$  are the frictional shear forces on the contact hinge of key blocks B and C,  $\text{kN/m}^2$ ;  $Z_C$  is the support force of collapsed gangue on key block C,  $\text{kN/m}^2$ ;  $a$  is the height of the contact surface between the rock block, m;  $l_1$  and  $l_2$  are the lengths of key blocks B and C, m, and it is generally believed that the mining-induced rock block cycle fracture caused by the cycle to pressure step is basically equal to  $l$  (Han 2021); and  $h$  is the thickness of the key rock block, m.

Repeated mining disturbances affect the horizontal thrust of the key block, and in general, the horizontal thrust decreases under a mining disturbance. Therefore,  $T_D$  is defined as the reduced value of the horizontal thrust of the key block under repeated mining,  $T_D > 0$ . The expression of the horizontal

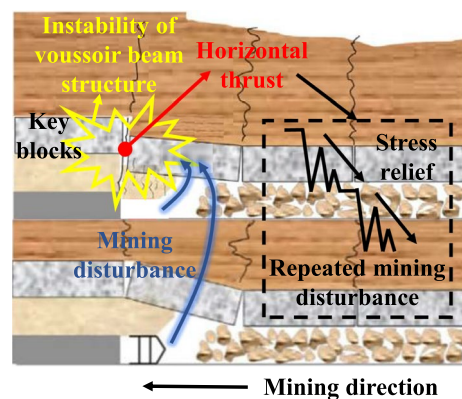
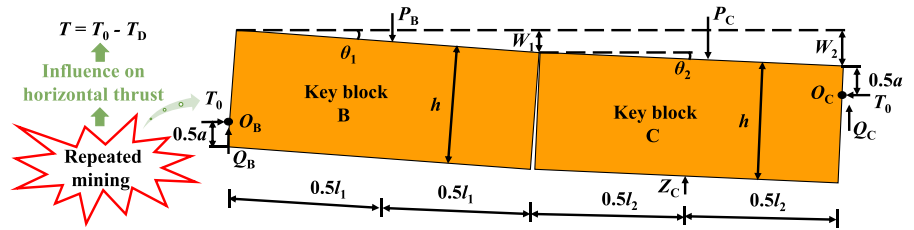


**Fig. 14** Schematic diagram of the instability of the VBS under repeated mining (Li et al. 2018)

**Fig. 15** Force analysis of the key blocks of the VBS under mining disturbances



thrust of the key block under repeated mining disturbances is shown in Eq. (8).

$$T = T_0 - T_D \tag{8}$$

where  $T$  is the horizontal thrust of key blocks under repeated mining disturbances,  $\text{kN/m}^2$ ;  $T_0$  is the initial horizontal thrust between rock blocks under single mining,  $\text{kN/m}^2$ ; and  $T_D$  is the reduced value of the horizontal thrust of the key block under repeated mining,  $\text{kN/m}^2$ .

In Fig. 15, the sinking amount ( $W_1$ ) of key block B is determined mainly by parameters such as the mining height ( $M$ ), the total thickness ( $\sum h$ ) of the direct top coal seam, and the fragmentation expansion coefficient ( $K_p$ ) when the rock block in the caved zone has just collapsed and initially stabilized. The calculation Equation is as follows.

$$W_1 = M - \sum h(K_p - 1) \tag{9}$$

From the contact geometry of the key rock block after rotation, it is known that the contact of both ends of the key rock block should be equal. Therefore, the contact surface height ( $a$ ) between the key rock block is calculated by using Eq. (10).

$$a = \frac{1}{2}(h - l_1 \sin \theta_1) = \frac{1}{2}(h - l \sin \theta_1) \tag{10}$$

Given that the contact between the key rock blocks is a plastic hinge relationship, the location of the initial horizontal thrust ( $T_0$ ) action point in Fig. 15 is taken as key block B at the height direction  $a/2$ . According to the equilibrium relationship of the key block mechanical model of the VBS shown in Fig. 15, the bending moment at point  $O_B$  is 0. Then, the following equation is available.

$$T_0 = \frac{l(P_B + P_C - Z_C)}{2(h + W_2 - 2W_1 - a)} \tag{11}$$

$$Q_C = (W_2 - W_1) \frac{l(P_B + P_C - Z_C)}{2l(h + W_2 - 2W_1 - a)} + \frac{1}{2}(P_C - Z_C) \tag{12}$$

From the geometric relationship,  $W_1 = l \sin \theta_1$ ,  $W_2 = l(\sin \theta_1 + \sin \theta_2) \sin \theta_1$  can be obtained. Then, let  $i = h/l$  denote the ratio of the height ( $h$ ) to the length ( $l$ ) of the key block, referred to as the key block fracture degree or block degree. According to the force analysis and calculation of the key block of the VBS, it can be approximated that  $P_C = Z_C$ ,  $\theta_2 \approx \theta_1/4$ . By further simplifying Eqs. (11) and (12), the following equation is obtained.

$$T_0 = \frac{P_B}{i - \frac{1}{2} \sin \theta_1} \tag{13}$$

$$Q_C = \frac{P_B \sin \theta_1}{2(2i - \sin \theta_1)} \tag{14}$$

According to the key block mechanics model of the VBS shown in Fig. 15, the equation of force equilibrium in the vertical direction is derived as  $Q_B = P_B - Q_C$ . Therefore, Eq. (15) can be obtained.

$$Q_B = \frac{(4i - 3 \sin \theta_1)P_B}{2(2i - \sin \theta_1)} \tag{15}$$

### 4.3 Stability criterion of the VBS under mining disturbances

Voussoir beam theory states that the stability of the VBS is mainly controlled by key rock blocks B and C in Fig. 15. The stability of the VBS in the fractured zone is mainly analyzed to determine the stability of the key rock block B and C structures. To maintain the stability of the structure, it is necessary to prevent the slip instability (S instability) that may be formed under a small angle of rotation ( $\theta_1$ ) when the hard key

strata is first fractured in Fig. 15 and to prevent the rotation instability (R instability) that may be formed when the angle of rotation ( $\theta_1$ ) gradually increases and leads to the crushing of the occlusion point (Li et al. 2018). The overlying strata VBS is stable only when the above two conditions are satisfied, which is the S-R stability criterion of the VBS (Han 2021). Therefore, the analysis of the stability of the overlying strata structure under repeated mining is based on the S-R stability criterion of the key blocks of the VBS and further analysis of whether repeated mining disturbances affect the S-R stability of the VBS in the overlying strata.

The maximum shear force ( $Q_B$ ) of the overlying strata VBS occurs at point  $O_B$ . To prevent the VBS from slipping and destabilizing at point  $O_B$  under repeated mining, the following conditions must be satisfied.

$$T \tan \varphi \geq Q_B \tag{16}$$

where  $\tan \varphi$  is the friction factor between key rock blocks, generally taken as 0.3 (Han 2021).

Substituting Eqs. (8), (13) and (15) into Eq. (16), the criterion of slip instability of the VBS under repeated mining disturbance can be obtained. Therefore, to ensure that the VBS does not produce slip instability under repeated mining disturbance, Eq. (17) must be satisfied.

$$T_D \leq \frac{(4 \tan \varphi - 4i - 3 \sin \theta_1) P_B}{2 \tan \varphi (2i - \sin \theta_1)} \tag{17}$$

From Eq. (17), the nonslip destabilization of the VBS under repeated mining is related to  $T_D$ ,  $i$ ,  $\theta_1$ ,  $P_B$  and  $\tan \varphi$ .

In addition, with the rotation of key block B (Fig. 15), the horizontal thrust can also cause rotation instability of key rock block B in the VBS. At this time, the condition to keep the VBS from rotational instability is Eq. (18).

$$T \leq a\eta R_C \tag{18}$$

where  $T/a$  is the average extrusion stress on the contact surface and  $\eta R_C$  is the extrusion strength of the rock block at the corner end, which is generally taken as 0.3 (Han 2021).

Substituting Eq. (13) and related parameters into Eq. (18) yields Eq. (19). To ensure that the VBS does

not produce rotation instability under repeated mining, Eq. (19) must be satisfied.

$$T_D \geq \frac{0.15 \left( i - \frac{1}{2} \sin \theta_1 \right) (h - l \sin \theta_1) R_C - P_B}{i - \frac{1}{2} \sin \theta_1} \tag{19}$$

From Eq. (19), whether the VBS under repeated mining experiences rotation instability is related to  $T_D$ ,  $i$ ,  $\theta_1$ ,  $P_B$  and  $R_C$ .

In summary, the overlying strata structure under repeated mining is still a VBS. The stability of the overlying strata is related to  $T_D$ ,  $i$ ,  $\theta_1$ ,  $P_B$ ,  $\tan \varphi$  and  $R_C$ . The S-R stability criterion of a VBS under repeated mining can be summarized as Eq. (20).

$$\left\{ \begin{array}{l} T_D \leq \frac{(4 \tan \varphi - 4i - 3 \sin \theta_1) P_B}{2 \tan \varphi (2i - \sin \theta_1)} \\ T_D \geq \frac{0.15 \left( i - \frac{1}{2} \sin \theta_1 \right) (h - l \sin \theta_1) R_C - P_B}{i - \frac{1}{2} \sin \theta_1} \end{array} \right. \tag{20}$$

Taking a mine as an engineering calculation example (Han 2021), its coal seam is approximately 48 m deep and 3 m thick. The overburden lithology of the roof of the longwall mining gob area is mainly interbedded sandstone and mudstone, and the comprehensive type of overburden is medium-hard overburden. The caved zone is approximately 10 m in height, and the fractured zone is approximately 28 m in height. The fractured zone runs from the bottom interface to the top interface and is underlain by a thick hard sandstone that acts as a bearer and contains a number of layers of soft mudstone or sandstone above. Among them, the lowermost group, close to the caved zone, with cavities below and most vulnerable to destabilization, consists of thick hard sandstone (i.e., key block B<sub>1</sub>). The key block is approximately 3 m thick, with a compressive strength of 35 MPa and an initial turnback angle of approximately 3°. The main roof cycle comes in pressure steps of approximately 30 m. According to the above derived criteria, assuming that there are still coal seam mining activities below the mining area and the horizontal thrust is reduced under the repeated mining, the value of each engineering calculation case is substituted into the S condition, and the condition that no slip destabilization

will occur is  $T_D \leq 7256 \text{ kN/m}^2$ . This means that the reduced value of the horizontal thrust of the key block under repeated mining is less than  $7256 \text{ kN/m}^2$  when the overlying strata remains stable. Conversely, when it is greater than  $7256 \text{ kN/m}^2$ , the VBS slips and becomes unstable, and the overlying strata becomes unstable. This shows that  $T_D$  has a greater influence on the stability of the overlying strata.

Notably, the S-R instability of the VBS is complex, and in this research, the experiments were carried out mainly from the effects of repeated mining disturbances on the stress unloading of fractured blocks.  $T_D$  was introduced based on the experimental results to obtain the S-R stability criterion of the VBS under repeated mining, which had certain limitations. For graded cyclic loading and unloading, different decreasing amplitudes and cycle parameters influence the results. Furthermore, the mechanical model of the VBS under repeated mining can be improved, and this study only considered the effect of mining disturbances on the horizontal thrust but not on the vertical stress. Therefore, these are potential areas for future research.

## 5 Conclusions

To investigate the mechanical characteristics of fractured blocks in the fractured zone, cyclic loading experiments of red sandstone at different ISL were carried out. The deformation parameters, energy evolution and damage characteristics of the red sandstone were investigated, which in turn provided some inspiration for the stability of the overlying strata. The main conclusions of this research are as follows.

- (1) In both the 1st and 2nd cyclic unloading stages, the elastic modulus showed a nonlinear decreasing trend as the number of cycles increased. The load-unload response ratio fluctuates at approximately 1. In addition, in the 1st unloading cycle, the irreversible strain was expressed in three stages: the initial rapid stage, the stable stage, and the accelerated stage of strain increase. In the 2nd cyclic unloading stage, the irreversible strain was only expressed in the two stages.
- (2) With increasing cycle number, the total strain energy showed a decreasing trend, and the elastic strain energy showed a smooth trend in gen-

eral, but part of the elastic strain energy showed a linear increasing trend. The evolution pattern of the dissipative strain energy and its proportion was similar to that of the input energy, showing a decreasing trend. This indicated that strain energy is a good indicator to characterize the damage. Therefore, the damage variable, based on the dissipation strain energy definition, showed a parabolic growth trend with increasing cycle number during the cyclic unloading stages. In addition, the irreversible strain and damage variables showed an “increasing–decreasing–increasing” trend as the ISL increased.

- (3) Based on the mechanical experimental results, the inspiration for the VBS in the overlying strata was derived. Based on the key block analysis method of the VBS mechanics model, the key block force analysis model of VBS stability under repeated mining was constructed. The calculation formula of the key block force of the VBS under repeated mining was derived. Combined with the S-R stability theory of key blocks of VBSs, the S-R stability criterion of these structures in the overlying strata under repeated mining disturbances was established.

**Acknowledgements** This work is financially supported by the National Key R&D Program of China (Grant No. 2022YFC3004704), the National Natural Science Foundation of China (Grant Nos. 52174166 and 52074041) and “Overall Rationing System” Project of Chongqing Talent Program (cst-c2022ycjh-bgzxm0077), which are gratefully acknowledged.

**Data availability** All data used during this research are available from the corresponding author by request.

### Declarations

**Competing interest** The authors declare no conflicts of interest.

**Open Access** This article is licensed under a Creative Commons Attribution 4.0 International License, which permits use, sharing, adaptation, distribution and reproduction in any medium or format, as long as you give appropriate credit to the original author(s) and the source, provide a link to the Creative Commons licence, and indicate if changes were made. The images or other third party material in this article are included in the article’s Creative Commons licence, unless indicated otherwise in a credit line to the material. If material is not included in the article’s Creative Commons licence and your intended use is not permitted by statutory regulation or exceeds

the permitted use, you will need to obtain permission directly from the copyright holder. To view a copy of this licence, visit <http://creativecommons.org/licenses/by/4.0/>.

## References

- Arora K, Chakraborty T, Rao KS (2019) Experimental study on stiffness degradation of rock under uniaxial cyclic sinusoidal compression loading. *Rock Mech Rock Eng* 52(11):4785–4797. <https://doi.org/10.1007/s00603-019-01835-3>
- Cerfontaine B, Collin F (2018) Cyclic and fatigue behaviour of rock materials: review, interpretation and research perspectives. *Rock Mech Rock Eng* 51(2):391–414. <https://doi.org/10.1007/s00603-017-1337-5>
- Chen YL, Zuo JP, Liu DJ, Li YJ, Wang ZB (2021) Experimental and numerical study of coal-rock bimaterial composite bodies under triaxial compression. *Int J Coal Sci Technol* 8(5):908–924. <https://doi.org/10.1007/s40789-021-00409-5>
- Dou LT, Yang K, Chi XL (2020) Fracture behavior and acoustic emission characteristics of sandstone samples with inclined precracks. *Int J Coal Sci Technol* 8(1):77–87. <https://doi.org/10.1007/s40789-020-00344-x>
- Duan MK, Jiang CB, Xing HL, Zhang DM, Peng K, Zhang WZ (2020) Study on damage of coal based on permeability and load-unload response ratio under tiered cyclic loading. *Arab J Geosci* 13(6):250. <https://doi.org/10.1007/s12517-020-5249-4>
- Feng LF, Dou LM, Wang XD, Jin DW, Cai W, Xu GG, Jiao B (2019) Mechanism of mining advance speed on energy release from hard roof movement. *J China Coal Soc* 44(11):3329–3339. <https://doi.org/10.13225/j.cnki.jccs.2018.1671>
- Feng XT, Gao YH, Zhang XW, Wang ZF, Zhang Y, Han Q (2020) Evolution of the mechanical and strength parameters of hard rocks in the true triaxial cyclic loading and unloading tests. *Int J Rock Mech Min Sci* 131:104349. <https://doi.org/10.1016/j.ijrmms.2020.104349>
- Fu B, Hu LH, Tang CA (2020) Experimental and numerical investigations on crack development and mechanical behavior of marble under uniaxial cyclic loading compression. *Int J Rock Mech Min Sci* 130:104289. <https://doi.org/10.1016/j.ijrmms.2020.104289>
- Gao YH, Feng XT (2019) Study on damage evolution of intact and jointed marble subjected to cyclic true triaxial loading. *Eng Fract Mech* 215:224–234. <https://doi.org/10.1016/j.engfracmech.2019.05.011>
- Gong FQ, Wu C, Luo S, Yan JY (2019a) Load-unload response ratio characteristics of rock materials and their application in prediction of rockburst proneness. *Bull Eng Geol Env* 78(7):5445–5466. <https://doi.org/10.1007/s10064-019-01474-6>
- Gong FQ, Yan JY, Luo S, Li XB (2019b) Investigation on the linear energy storage and dissipation laws of rock materials under uniaxial compression. *Rock Mech Rock Eng* 52(11):4237–4255. <https://doi.org/10.1007/s00603-019-01842-4>
- Han KM (2021) Mechanical analysis of instability of overburden structure in goaf under surface load. *J China Coal Soc* 46(S1):10–16
- Hao XJ, Du WS, Zhao YX, Sun ZW, Zhang Q, Wang SH, Qiao HQ (2020) Dynamic tensile behaviour and crack propagation of coal under coupled static-dynamic loading. *Int J Min Sci Technol* 30(5):659–668. <https://doi.org/10.1016/j.ijmst.2020.06.007>
- Kong B, Wang EY, Li ZH, Wang XR, Chen L, Kong XG (2016) Nonlinear characteristics of acoustic emissions during the deformation and fracture of sandstone subjected to thermal treatment. *Int J Rock Mech Min Sci* 90:43–52. <https://doi.org/10.1016/j.ijrmms.2016.10.004>
- Le JL, Manning J, Labuz JF (2014) Scaling of fatigue crack growth in rock. *Int J Rock Mech Min Sci* 72:71–79. <https://doi.org/10.1016/j.ijrmms.2014.08.015>
- Li XB, Gong FQ, Tao M, Dong LJ, Du K, Ma CD, Zhou ZL, Yin TB (2017) Failure mechanism and coupled static-dynamic loading theory in deep hard rock mining: a review. *J Rock Mech Geotech Eng* 9(4):767–782. <https://doi.org/10.1016/j.jrmge.2017.04.004>
- Li Z, Xu JL, Ju JF, Zhu WB, Xu JM (2018) The effects of the rotational speed of voussoir beam structures formed by key strata on the ground pressure of stopes. *Int J Rock Mech Min Sci* 108:67–79. <https://doi.org/10.1016/j.ijrmms.2018.04.041>
- Li QM, Liang YP, Zou QL, Li QG (2020) Acoustic emission and energy dissipation characteristics of gas-bearing coal samples under different cyclic loading paths. *Nat Resour Res* 29(2):1397–1412. <https://doi.org/10.1007/s11053-019-09508-2>
- Liang YP, Li B, Yuan Y, Zou QL, Jia LX (2017) Moving type of key strata and its influence on ground pressure in fully mechanized mining face with large mining height. *J China Coal Soc* 42(06):1380–1391
- Liang YP, Ran QC, Zou QL, Zhang BC, Hong Y (2022) Experimental study of mechanical behaviors and failure characteristics of coal under true triaxial cyclic loading and unloading and stress rotation. *Nat Resour Res* 31(2):971–991. <https://doi.org/10.1007/s11053-022-10022-1>
- Liu Y, Dai F, Dong L, Xu NW, Feng P (2018) Experimental investigation on the fatigue mechanical properties of intermittently jointed rock models under cyclic uniaxial compression with different loading parameters. *Rock Mech Rock Eng* 51(1):47–68. <https://doi.org/10.1007/s00603-017-1327-7>
- Liu XL, Liu Z, Li XB, Gong FQ, Du K (2020) Experimental study on the effect of strain rate on rock acoustic emission characteristics. *Int J Rock Mech Min Sci* 133:104420. <https://doi.org/10.1016/j.ijrmms.2020.104420>
- Liu B, Zhao YX, Zhang C, Zhou JL, Li YT, Sun Z (2021) Characteristic strength and acoustic emission properties of weakly cemented sandstone at different depths under uniaxial compression. *Int J Coal Sci Technol* 8(6):1288–1301. <https://doi.org/10.1007/s40789-021-00462-0>
- Meng QB, Wang CK, Liu JF, Zhan MW, Lu MM, Wu Y (2020) Physical and micro-structural characteristics of limestone after high temperature exposure. *Bull Eng Geol Env* 79(3):1259–1274. <https://doi.org/10.1007/s10064-019-01620-0>



- Meng QB, Liu JF, Ren L, Pu H, Chen YL (2021a) Experimental study on rock strength and deformation characteristics under triaxial cyclic loading and unloading conditions. *Rock Mech Rock Eng* 54(2):777–797. <https://doi.org/10.1007/s00603-020-02289-8>
- Meng QB, Liu JF, Pu H, Yu LY, Wu JY, Wang CK (2021b) Mechanical properties of limestone after high-temperature treatment under triaxial cyclic loading and unloading conditions. *Rock Mech Rock Eng* 54(12):6413–6437. <https://doi.org/10.1007/s00603-021-02638-1>
- Peng K, Zhou JQ, Zou QL, Yan FZ (2019a) Deformation characteristics of sandstones during cyclic loading and unloading with varying lower limits of stress under different confining pressures. *Int J Fatigue* 127:82–100. <https://doi.org/10.1016/j.ijfatigue.2019.06.007>
- Peng K, Liu ZP, Zou QL, Zhang ZY, Zhou JQ (2019b) Static and dynamic mechanical properties of granite from various burial depths. *Rock Mech Rock Eng* 52(10):3545–3566. <https://doi.org/10.1007/s00603-019-01810-y>
- Peng K, Zhou JQ, Zou QL, Zhang YJ, Tan GW (2020) Deformation characteristics and failure modes of sandstones under discontinuous multi-level cyclic loads. *Powder Technol* 373:599–613. <https://doi.org/10.1016/j.powtec.2020.06.076>
- Qu QD, Xu JL, Wu RL, Qin W, Hu GZ (2015) Three-zone characterisation of coupled strata and gas behaviour in multi-seam mining. *Int J Rock Mech Min Sci* 78:91–98. <https://doi.org/10.1016/j.ijrmms.2015.04.018>
- Renani HR, Cai M (2021) Forty-year review of the Hoek-Brown failure criterion for jointed rock masses. *Rock Mech Rock Eng* 55(1):439–461. <https://doi.org/10.1007/s00603-021-02661-2>
- Suchowerska AM, Carter JP, Merifield RS (2014) Horizontal stress under supercritical longwall panels. *Int J Rock Mech Min Sci* 70:240–251. <https://doi.org/10.1016/j.ijrmms.2014.03.009>
- Tian WL, Yang SQ, Wang JG, Dong JP (2021) Failure behavior of the thermal treated granite under triaxial cyclic loading-unloading compression. *Geomech Geophys Geo-Energy Geo-Resour* 7(1):19. <https://doi.org/10.1007/s40948-021-00218-9>
- Wang Y, Gao SH, Li CH, Han JQ (2020) Investigation on fracture behaviors and damage evolution modeling of freeze-thawed marble subjected to increasing- amplitude cyclic loads. *Theor Appl Fract Mech* 109:102679. <https://doi.org/10.1016/j.tafmec.2020.102679>
- Wang Y, Han JQ, Ren JY, Li CH (2021) Anisotropic fracture and energy dissipation characteristics of interbedded marble subjected to multilevel uniaxial compressive cyclic loading. *Fatigue Fract Eng M* 44(2):366–382. <https://doi.org/10.1111/ffe.13365>
- Wei P, Li XL, Hu QT, Peng SJ, Liu S (2020) A trapezoidal three-dimensional model for gas extraction based on shapes of caved overlying strata and numerical calculation. *Nat Resour Res* 29(6):4031–4051. <https://doi.org/10.1007/s11053-020-09677-5>
- Whittles DN, Lowndes IS, Kingman SW, Yates C, Jobling S (2007) The stability of methane capture boreholes around a long wall coal panel. *Int J Coal Geol* 71(2–3):313–328. <https://doi.org/10.1016/j.coal.2006.11.004>
- Wu XM, Li GD, Luo F, Duan S (2021) A study on the distribution and evolution of mining induced stress under the condition of multiple mining. *Geotech Geol Eng* 39(2):1637–1648. <https://doi.org/10.1007/s10706-020-01582-1>
- Xia Z, Yao QL, Meng GS, Xu Q, Tang CJ, Zhu L, Wang WN, Shen Q (2021) Numerical study of stability of mining roadways with 6.0-m section coal pillars under influence of repeated mining. *Int J Rock Mech Min Sci* 138:104641. <https://doi.org/10.1016/j.ijrmms.2021.104641>
- Xiao F, Jiang DY, Wu F, Zou QL, Chen J, Chen B, Sun ZG (2020) Effects of prior cyclic loading damage on failure characteristics of sandstone under true-triaxial unloading conditions. *Int J Rock Mech Min Sci* 132:104379. <https://doi.org/10.1016/j.ijrmms.2020.104379>
- Yang SQ (2016) Experimental study on deformation, peak strength and crack damage behavior of hollow sandstone under conventional triaxial compression. *Eng Geol* 213:11–24. <https://doi.org/10.1016/j.enggeo.2016.08.012>
- Zhang J, Wang B (2021) Study on the bearing structure and stability of overlying strata: an interval gob in shallow buried coal mining of Northwest China. *Arab J Geosci* 14(4):255. <https://doi.org/10.1007/s12517-021-06479-8>
- Zhang BC, Sun HT, Liang YP, Wang KQ, Zou QL (2019a) Characterization and quantification of mining-induced fractures in overlying strata: implications for coalbed methane drainage. *Nat Resour Res* 29(4):2467–2480. <https://doi.org/10.1007/s11053-019-09600-7>
- Zhang P, Gearhart D, Van Dyke M, Su D, Esterhuizen E, Tulu B (2019b) Ground response to high horizontal stresses during longwall retreat and its implications for longwall headgate support. *Int J Min Sci Technol* 29(1):27–33. <https://doi.org/10.1016/j.ijmst.2018.11.020>
- Zhang C, Bai QS, Chen YH (2020) Using stress path-dependent permeability law to evaluate permeability enhancement and coalbed methane flow in protected coal seam: a case study. *Geomech Geophys Geo-Energy Geo-Resour* 6(3):53. <https://doi.org/10.1007/s40948-020-00177-7>
- Zhang TC, Zou QL, Jia XQ, Liu T, Jiang ZB, Tian SX, Jiang CZ, Cheng YY (2022a) Effect of cyclic water injection on the wettability of coal with different SiO<sub>2</sub> nanofluid treatment time. *Fuel* 312:122922. <https://doi.org/10.1016/j.fuel.2021.122922>
- Zhang P, Esterhuizen G, Sears M, Trackemas J, Minoski T, Tulu B (2022b) Roof stability and support strategies associated with longwall-induced horizontal stress changes in belt entries. *Min Metal Explor*. <https://doi.org/10.1007/s42461-022-00634-9>
- Zhang BC, Liang YP, Zou QL, Ding LQ (2022c) Determination of crack closure stress under constant-fatigue loading based on damage variable evolution. *Theor Appl Fract Mech* 121:103526. <https://doi.org/10.1016/j.tafmec.2022c.103526>
- Zhao YH, Wang SR, Zou ZS, Ge LL, Cui F (2018) Instability characteristics of the cracked roof rock beam under shallow mining conditions. *Int J Min Sci Technol* 28(3):437–444. <https://doi.org/10.1016/j.ijmst.2018.03.005>
- Zhao HG, Song ZL, Zhang DM, Liu C, Yu BC (2021a) True triaxial experimental study on mechanical characteristics and energy evolution of sandstone under various loading and unloading rates. *Geomech Geophys*

- Geo-Energy Geo-Resour 7(1):22. <https://doi.org/10.1007/s40948-020-00212-7>
- Zhao Y, Bi J, Wang CL, Liu PF (2021b) Effect of unloading rate on the mechanical behavior and fracture characteristics of sandstones under complex triaxial stress conditions. *Rock Mech Rock Eng* 54(9):4851–4866. <https://doi.org/10.1007/s00603-021-02515-x>
- Zhao PX, Wang JN, Li SG, Li H, Qin L, Lin HF, Shu CM, Bin LW, Jia YY, Wei ZY, Pei WB (2022) Effects of recovery ratio on the fracture evolution of the overburden pressure-relief gas migration channel for a fully mechanized working face. *Nat Resour Res* 31(2):1011–1026. <https://doi.org/10.1007/s11053-021-09993-4>
- Zhu WC, Li SH, Li S, Niu LL (2019) Influence of dynamic disturbance on the creep of sandstone: an experimental study. *Rock Mech Rock Eng* 52(4):1023–1039. <https://doi.org/10.1007/s00603-018-1642-7>
- Zhu XY, Chen XD, Dai F (2020) Mechanical properties and acoustic emission characteristics of the bedrock of a hydropower station under cyclic triaxial loading. *Rock Mech Rock Eng* 53(11):5203–5221. <https://doi.org/10.1007/s00603-020-02218-9>
- Zou QL, Liu H, Jiang ZB, Wu X (2021) Gas flow laws in coal subjected to hydraulic slotting and a prediction model for its permeability-enhancing effect. *Energy Sour Part a-Recov Util Environ Effects*. <https://doi.org/10.1080/15567036.2021.1936692>
- Zou QL, Zhang TC, Ma TF, Tian SX, Jia XQ, Jiang ZB (2022a) Effect of water-based SiO<sub>2</sub> nanofluid on surface wettability of raw coal. *Energy* 254:124228. <https://doi.org/10.1016/j.energy.2022a.124228>
- Zou QL, Zhou XL, Wang RZ, Ning YH, Chen ZH, Kong FJ, Liu Y (2022b) Load-carrying and energy-absorbing performance of honeycombs with different cross sections under cyclic loading. *Mater Today Commun* 33:104582. <https://doi.org/10.1016/j.mtcomm.2022b.104582>

**Publisher's Note** Springer Nature remains neutral with regard to jurisdictional claims in published maps and institutional affiliations.